

# Stability analysis of flow of active extensile fibers in confined domains

M. Carme Calderer,<sup>1</sup> Dmitry Golovaty,<sup>2</sup> Lingxing Yao,<sup>2</sup> Jordi Ignès Mallol,<sup>3</sup> Longhua Zhao,<sup>4</sup> and Francesc Sagués<sup>3</sup>

<sup>1</sup>*School of Mathematics, University of Minnesota*

<sup>2</sup>*Department of Mathematics, University of Akron*

<sup>3</sup>*Department of Chemistry, University of Barcelona*

<sup>4</sup>*Department of Mathematics, Applied Mathematics and Statistics, Case Western Reserve University*

We study the shear flow of active extensile filaments confined in a thin channel. We apply the Ericksen-Leslie equations of liquid crystal flow with an activity source term. The dimensionless form of this system includes the Ericksen, Activity and Reynolds numbers, together with the aspect ratio of the channel, as the main driving parameters. We perform a normal mode stability analysis of the base shear flow. We arrive at a comprehensive description of the stability properties and their dependence on the parameters of the system. The transition to instability occurs at a positive threshold value of the activity parameter. The work is guided by experiments on active filaments in confined channels and aims at quantifying their findings in the prechaotic regime.

**This article presents a comprehensive stability analysis of the aligning shear flow of active fibers driven by biological fuel. The study cover both extensile and contractile fibers confined in narrow channels. Both types of materials are serving as controlled experimental model relevant to biological and medical discoveries, with the contractile ones being used in simulating actin filaments in cells. And for extensile fibers, we closely follow experiments of microtubules as reported in the recent articles. In our study, to make predictions for experiments in either cases, the activity level, the ratio of the viscous to the elastic torques, and the channel geometry are quantitatively characterized as the mechanisms that trigger instability, and their role on the vorticity profiles of the perturbing flow is analyzed. Particularly, it is found that contractile fibers are very sensitive to the Reynolds number of the flow, which reveal possible signatures of plastic behavior. To conduct stability analysis, the spectral method is used to solve the generalized eigenvalue problems arising in the analysis.**

## I. INTRODUCTION

We study laminar flow of active extensile filaments confined to thin channels. Our flow model is based on the Ericksen-Leslie equations of liquid crystals with an added activity source term (<sup>12,11</sup>). We analyze the mechanisms of instability of well-aligned shear flows with linear velocity profile and quantitatively explore regimes of instability. We perform a normal mode analysis of the flow equations and find the instability thresholds of the uniformly aligned shear flow in terms of the relevant nondimensional parameter groups. Increased activity and Ericksen number are found to drive the system out of the stable regime. We also find that the vorticity and speed of the perturbing flow increase as the activity number  $\mathcal{A}$  increases. A numerical method based on the discretization of the linear system by Chebyshev polynomials is used in the stability analysis, specifically, in solving the underlying spectral problem. The outcome provides a comprehensive description of the stability profiles of the fibers in confinement, in terms of the activity, Ericksen and Reynolds numbers, and the geometry of the channel.

Extensile fibers are known to form rodlike nematic liquid crystalline phases, due to their elongated molecular shapes. The material that we study consists of self-propelled elongated fiber units formed by bundled microtubules that are powered by adenosine triphosphate (ATP)-consuming kinesin 29<sup>16</sup>. Our results show very good agreement with the laboratory experimental studies by the Catalan group<sup>10</sup>, aimed at understanding the behavior of active matter in confinement.

The study of active matter in confinement is very relevant to understanding many biological systems as well as in guiding potential applications. In contrast with passive systems, whose dynamics is the direct result of external agents (e.g., a pump in Poiseuille flow), active matter systems are able to use stored energy or extract it from external sources at small (or at *individual*) length scales and collectively enhance it at the macroscopic scale—often in cooperation with the environment (e.g. bacteria swimming in a liquid crystal media)—and convert it into work<sup>13,15</sup>. Typical examples of these systems include bacteria in either isotropic or liquid crystal media, cytoplasm networks, and cancer cells.

The aim of our work is to provide theoretical support to recent experiments of shear flow of extensile fibers in confined channels of varying width in order to understand complex phenomenology of active flow in a controlled setting<sup>10</sup>. Earlier theoretical work on extensile fibers found that laterally confined active nematics undergo an instability of a spontaneous laminar flow when the channel width reaches a certain threshold value that depends on the strength of the activity<sup>20</sup>. These results were later confirmed in experiments with spindle-shaped cells<sup>5</sup>.

The Ericksen-Leslie equations of incompressible liquid crystal flow and their numerical simulations have been used in many studies of active systems, especially in the turbulent regimes<sup>9</sup>. The variables of the model include the velocity field  $\mathbf{v}$ , the pressure  $p$  associated with the incompressibility constraint and the unit nematic director  $\mathbf{n}$ , representing the local average alignment of the system. Since the flows that we study are plane, we formulate the problem in terms of the *stream function*  $\Psi$ .

The dimensionless form of the equations involves, in addition to the aspect ratio  $\ell$  of the channel, three main parameter groups. Two of them—the Reynolds  $\mathcal{R}_e$  and Ericksen  $\mathcal{E}_r$  numbers—are defined in the same way as for passive flows. The activity parameter  $\mathcal{A}$  quantifies the activity level in the system. Although  $\mathcal{R}_e$  is significantly smaller than other nondimensional parameters influences the stability behavior of the active system in some saddle ways. The  $\mathcal{E}_r$  represents the ratio of the viscous to the elastic torques and may take very large values.

In this work, we focus on the plane shear flow of an active liquid crystal in the aligning regime. We find solutions with linear velocity profiles and constant angles of alignment that agree with experimental observations of active filaments in a channel when  $\mathcal{A} > 0$ <sup>10</sup>. We also find a velocity gradient of equal magnitude but opposite sign for the flow of contractile fibers. Aligning regimes are characterized by the dominance of the extensional effect of the shear flow over the rotating one, as characterized by the value  $|\lambda| > 1$  of the shear aligning parameter (for tumbling regimes  $|\lambda| < 1$ ). The dominance of the extensional effect causes the liquid crystal to align at a certain angle with respect to the direction of the velocity. Moreover  $\lambda > 0$  for extensile systems. We find that the magnitude of the velocity gradient is proportional to the activity parameter, and the angle of alignment solely depends on the ratio of two relevant anisotropic viscosity coefficients, as in the case of a passive shear flow.

Several works on active liquid crystals found in the literature use the Beris-Edwards model based on the evolution of the order tensor  $Q$  rather than the director of the Ericksen-Leslie theory<sup>6</sup>.  $Q$  represents a symmetric, traceless second order tensor whose two independent eigenvectors are the director fields of the theory. They reduce to a single eigenvector  $\mathbf{n}$  in the uniaxial case, with  $Q$  admitting the representation  $Q = s(\mathbf{n} \otimes \mathbf{n} - \frac{1}{3}I)$ , where the scalar  $s \in (-\frac{1}{2}, 1)$  corresponds to the single, independent eigenvalue. For rodlike liquid crystals,  $s > 0$ .

We carry out a normal mode analysis of the shear flow, with  $\omega$  representing the spatial frequency of the perturbation and  $\text{Im}(c)$  the corresponding growth rate. A perturbation with frequency  $\omega$  and  $\text{Im}(c) > 0$  is unstable, and otherwise, stable. The threshold  $\text{Im}(c) = 0$  represents neutral stability. We choose boundary conditions so that the boundary values of the base flow are not altered. The zero boundary conditions on perturbations suggest that a discretization using Chebyshev polynomials is appropriate. We apply the Chebyshev-QZ-algorithm to solve the generalized eigenvalue problem resulting from the linearization of the governing system about the base shear flow. We emphasize the secondary role of the director field boundary conditions. Indeed, one important difference between active and passive liquid crystals is that whereas the latter can be aligned by surface anchoring, this is not the case for active flows, known to respond to alignment by flow only.

The stability plots in the  $\mathcal{A}\omega$ -plane indicate positive threshold value of  $\mathcal{A}$  at which the system becomes unstable. This critical value decreases with increasing values of  $\mathcal{E}_r$  and  $\ell$ , and with the range of unstable frequencies also increasing. The growth rate profile calculated with respect to  $\mathcal{A}$  shows a parabolic profile for low frequencies becoming linear at a threshold frequency. The profile of  $\text{Im}(c)$  with respect to  $\omega$  starts being positive for all values of  $\mathcal{A}$ , reaching zero growth at a threshold value of  $\omega$  that appears to be independent of  $\mathcal{A}$ . With further increase of  $\omega$ ,  $\text{Im}(c)$  reaches a positive maximum, subsequently tending to zero as  $\omega$  increases, feature that is also independent of  $\mathcal{A}$ . These trends have been reported in the experimental literature<sup>10</sup>.

This paper is organized as follows. Section II presents the formulation of the Ericksen-Leslie system for active liquid crystals, including the assumptions that lead to aligning flows and a description of the boundary conditions. The scaling of the problem and non-dimensionalization of the equations are presented in Section III. The shear flow geometry and calculation of the corresponding steady states are presented in Section IV. The framework for the stability analysis is developed in Section V. The numerical method to analyze the stability of shear flows is presented in Section VI. In Section VII, we present the stability results. In section VIII, we present the conclusions.

The fully developed equations for the Ericksen-Leslie and Ericksen models are presented in the Supplementary Materials section. A summary of the plots that resulted from the numerical simulations is also given there.

## II. ACTIVE LIQUID CRYSTALS: THE ERICKSEN-LESLIE EQUATIONS

As for its passive counterpart, an active liquid crystal is assumed to be a viscous anisotropic and incompressible fluid with activity sources drawn from internal mechanisms or from the environment. Let  $\Omega \subset \mathbb{R}^3$  be an open domain occupied by the liquid crystal with the smooth boundary  $\partial\Omega$ . The Ericksen-Leslie equations of balance of linear and angular momentum, and the incompressibility and unit director constraints for the velocity field  $\mathbf{v}$ , pressure  $p$  and

director field  $\mathbf{n}$  in  $\Omega$  and at time  $t > 0$  are<sup>11</sup>:

$$\rho \dot{\mathbf{v}} = \nabla \cdot \boldsymbol{\sigma}, \quad (1)$$

$$\gamma_1 \dot{\mathbf{n}} \times \mathbf{n} = \nabla \cdot \left( \frac{\partial W_{\text{OF}}}{\partial \nabla \mathbf{n}} \right) \times \mathbf{n} - \frac{\partial W_{\text{OF}}}{\partial \mathbf{n}} \times \mathbf{n} + \gamma_1 \boldsymbol{\Omega} \mathbf{n} \times \mathbf{n} - \gamma_2 \mathbf{A} \mathbf{n} \times \mathbf{n}, \quad (2)$$

$$\nabla \cdot \mathbf{v} = 0, \quad (3)$$

$$\mathbf{n} \cdot \mathbf{n} = 1, \quad (4)$$

with  $\rho > 0$  denoting the constant mass density. We point out that, since the system is strongly dissipative, rotational inertia has been neglected in equation (2). Moreover, such an equation results from taking the cross product of the original equation of balance of angular momentum by the vector  $\mathbf{n}$ . This has the advantage of explicitly suppressing the Lagrange multiplier associated with the unit director field constraint. The function  $W_{\text{OF}}$  denotes the Oseen-Frank energy of the liquid crystal, quadratic in the gradients of  $\mathbf{n}$ :

$$W_{\text{OF}}(\mathbf{n}, \nabla \mathbf{n}) = \frac{1}{2} (k_1 |\nabla \cdot \mathbf{n}|^2 + k_2 |(\nabla \times \mathbf{n}) \cdot \mathbf{n}|^2 + k_3 |(\nabla \times \mathbf{n}) \times \mathbf{n}|^2 + (k_2 + k_4) \nabla \cdot [(\mathbf{v} \cdot \nabla) \mathbf{n} - (\nabla \cdot \mathbf{n}) \mathbf{n}]). \quad (5)$$

with  $k_1, k_2, k_3 > 0$ ,  $k_2 > |k_4|$  and  $2k_1 \geq k_2 + k_4$  denote the Frank elastic constants. The total energy is

$$\mathcal{E} = \int_{\Omega} \left( \frac{1}{2} \rho \dot{\mathbf{v}} \cdot \dot{\mathbf{v}} + W_{\text{OF}}(\mathbf{n}, \nabla \mathbf{n}) \right) dx.$$

The Cauchy stress tensor  $\boldsymbol{\sigma}$  is the sum of the elastic, viscous  $\hat{\boldsymbol{\sigma}}$  and active  $\boldsymbol{\sigma}_A$  components, respectively.

$$\boldsymbol{\sigma} = -p \mathbf{I} - \nabla \mathbf{n}^T \frac{\partial W_{\text{OF}}}{\partial \nabla \mathbf{n}} + \hat{\boldsymbol{\sigma}} + \boldsymbol{\sigma}_A, \quad (6)$$

$$\hat{\boldsymbol{\sigma}} = \alpha_1 (\mathbf{n} \cdot \mathbf{A} \mathbf{n}) \mathbf{n} \otimes \mathbf{n} + \alpha_2 \mathbf{N} \otimes \mathbf{n} + \alpha_3 \mathbf{n} \otimes \mathbf{N} + \alpha_4 \mathbf{A} + \alpha_5 \mathbf{A} \mathbf{n} \otimes \mathbf{n} + \alpha_6 \mathbf{n} \otimes \mathbf{A} \mathbf{n}, \quad (7)$$

$$\boldsymbol{\sigma}_A = -a \mathbf{n} \otimes \mathbf{n}, \quad (8)$$

where

$$2\mathbf{A} = \nabla \mathbf{v} + (\nabla \mathbf{v})^T, \quad 2\boldsymbol{\Omega} = \nabla \mathbf{v} - (\nabla \mathbf{v})^T \text{ and } \mathbf{N} = \dot{\mathbf{n}} - \boldsymbol{\Omega} \mathbf{n}.$$

Here the superimposed dot denotes the material time derivative, that is,  $\dot{f}(t, \mathbf{x}) = \frac{\partial f}{\partial t} + (\mathbf{v} \cdot \nabla) f$ . The Leslie coefficients  $\alpha_i$ ,  $1 \leq i \leq 6$  represent the anisotropic viscosities of the liquid crystal. In particular,  $\alpha_4$  corresponds to the isotropic or Newtonian viscosity. The parameter  $a$  in (8) quantifies the activity of the system, with  $a = 0$  corresponding to the standard Ericksen-Leslie system for passive liquid crystals.

The active part (8) of the stress tensor accounts for the non-conservative forces generated by the individual fibers and are assumed to be dipolar. Their expressions were obtained from the symmetry of the flow field that they generate, with  $a > 0$  corresponding to the extensile regime, and  $a < 0$  to the contractile one<sup>15,14,13,7</sup> as illustrated in figure 1. In the terminology of *swimmers*, extensile particles are known as *pushers* and contractile ones as *pullers*.

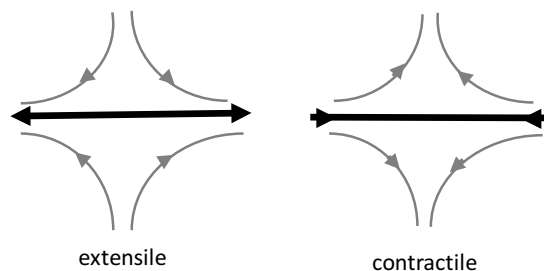


FIG. 1. Flow profile (grey curves) generated by extensile (left) and contractile fibers (right). The thick black arrow represents the nematic director, pointing along the rod axis in rodlike particles, and perpendicular to the disk in discotic ones.

### A. The Leslie coefficients and the dissipativeness of the system

The rate of dissipation function is quadratic on the time-rate quantities and takes the form

$$\Delta = \frac{1}{2} (\alpha_1 (\mathbf{n}^T \mathbf{A} \mathbf{n})^2 + \gamma_1 |\mathbf{N}|^2 + (\alpha_5 + \alpha_6) |\mathbf{A} \mathbf{n}|^2 + (\alpha_3 + \alpha_2 + \gamma_2) \mathbf{N}^T \mathbf{A} \mathbf{n} + \alpha_4 |\mathbf{A}|^2). \quad (9)$$

The second law of thermodynamics in the form of the Clausius-Duhem inequality reduces to the positivity of the rate of dissipation function,  $\Delta \geq 0$ . Necessary and sufficient conditions for the latter result in the well-known inequalities<sup>11</sup>:

$$\begin{aligned} \alpha_4 &> 0, \\ \alpha_1 + \frac{3}{2} \alpha_4 + \alpha_5 + \alpha_6 &> 0, \\ 2\alpha_4 + \alpha_5 + \alpha_6 - \frac{\gamma_2^2}{\gamma_1} &> 0, \\ \gamma_1 &:= \alpha_3 - \alpha_2 > 0, \\ \gamma_2 &:= \alpha_6 - \alpha_5. \end{aligned} \quad (10)$$

Parodi's relation, a consequence of Onsager's reciprocal relations in the microscale description of liquid crystals, is an additional assumption of the theory:

$$\alpha_6 - \alpha_5 = \alpha_2 + \alpha_3. \quad (11)$$

This condition renders the rate of dissipation function of a potential for the viscous stress, that is  $\hat{\sigma} = \frac{\partial \Delta}{\partial \nabla \mathbf{v}}$ . We consider a class of liquid crystals able to align under the effect of flow of small velocity gradient. This requires that

$$\left| \frac{\gamma_1}{\gamma_2} \right| := \frac{1}{\lambda} \leq 1, \quad (12)$$

$\lambda$  known as the flow alignment parameter. It represents the ratio between the extensional and rotational effects of the shear flow, with the former dominating in the case  $\lambda > 1$  and so the director aligns along the flow direction. The tumbling regime corresponds to  $\lambda < 1$ , with a prevailing rotational couple that prevents  $\mathbf{n}$  from choosing an aligning direction<sup>1,7</sup>. Moreover for extensile liquid crystals

$$\gamma_2 < 0. \quad (13)$$

(For disk-like, compressible liquid crystals,  $\gamma_2 > 0$ .)

### B. Boundary conditions

The behavior of active liquid crystals on the domain boundary may be significantly different from that of their passive counterparts. Whereas actin fibers may anchor and stick to the boundary, some active liquid crystals, such as microtubules, do not align by anchoring on the boundary and can only become oriented by flow. There is no evidence of non-slip behavior in experiments where microtubules are found to slide along the walls. Guided by experiments, slip-free boundary conditions were used in numerical simulations in<sup>10</sup>. Hence, we require

$$\mathbf{v} \cdot \boldsymbol{\nu} = 0, \quad \text{on } \partial\Omega, \quad (14)$$

$$(\boldsymbol{\sigma} \boldsymbol{\nu}) \cdot \boldsymbol{\tau} = 0, \quad (15)$$

where  $\boldsymbol{\nu}$  and  $\boldsymbol{\tau}$  denote the outer unit normal and tangent vectors to the boundary, respectively. For the director field, we impose zero Neumann boundary conditions:

$$\frac{d\mathbf{n}}{d\boldsymbol{\nu}} = 0 \quad \text{on } \partial\Omega. \quad (16)$$

When  $\Omega$  is a semi-infinite stripe domain with thickness  $2L_3$ , suppose that the flow and director field are restricted to the  $xz$ -plane, and denote by  $\phi$  the angle between  $\mathbf{n}$  and the  $z$ -axis. Then the conditions (14)-(16) become

$$v_2(x, -L_3) = v_3(x, L_3) = 0, \quad (17)$$

$$\sigma_{13} = 0, \quad (18)$$

$$\frac{d\phi}{d\nu} = 0, \quad (19)$$

respectively.

**Remark.** In the calculations for the stability analysis, we impose Dirichlet boundary conditions on the perturbation angle rather than the Neumann condition (19). This has been done to simplify the stability analysis but one would naturally expect different results for other boundary conditions.

### III. SCALING AND NON-DIMENSIONALIZATION

Next, we formulate the governing equations in terms of dimensionless time and space variables. For this, we choose the positive quantities  $L_1$  and  $L_3$  to be the characteristic lengths along the  $x$  and  $z$  directions, respectively, and let  $V > 0$  denote the characteristic velocity. Moreover, we take the isotropic coefficient  $\alpha_4$  to be the characteristic viscosity of the system, and let  $p_0 > 0$  represent the typical pressure. The resulting dimensionless variables are

$$\tilde{x} = \frac{x}{L_1}, \quad \tilde{z} = \frac{z}{L_3}, \quad \tilde{v}_1 = \frac{v_1}{V}, \quad \tilde{v}_3 = \frac{v_3}{V}, \quad \tilde{t} = \frac{t}{T}, \quad T = \frac{L_1}{V}, \quad \tilde{p} = \frac{p}{p_0}, \quad p_0 = \frac{V\eta}{L_1}. \quad (20)$$

The quantity  $T > 0$  represents the typical time scale. We subsequently, divide the governing equations, term by term, by the expression  $\alpha_4 \frac{V}{L_1^2}$ . The resulting equations involve well-known dimensionless parameter groups: the Reynolds number  $\text{Re}$ , the Ericksen number  $\mathcal{E}_r$  and the activity parameter  $\mathcal{A}$ , as well as the aspect ratio of the channel,  $\ell$ . The quantity  $\mathcal{E}_r$  represents the ratio of the viscous to the elastic torques. Further, we multiply the equation of balance of angular momentum by  $\frac{L_1^2}{k_1^2}$  which also brings  $\mathcal{E}_r$  into the expression.

We also need the following nondimensional parameters

$$\tilde{\alpha}_i = \frac{\alpha_i}{\rho VL}, \quad \tilde{\gamma}_i = \frac{\gamma_i}{\rho VL}, \quad \tilde{k} = \frac{k}{\rho V^2 L^2}, \quad (21)$$

where  $\tilde{\alpha}_i$  and  $\tilde{\gamma}_i$  are the dimensionless viscosity coefficients and  $\tilde{k}$  is the dimensionless elastic modulus. The list of the dimensionless parameters groups of the model is

$$\begin{aligned} \mathcal{R}_e &= \frac{L_1 V \rho}{\eta} : \text{Reynolds number,} \\ \mathcal{E}_r &= \frac{\eta L_1 V}{k} : \text{Ericksen number,} \\ \mathcal{A} &= \frac{a L_1}{V \eta} : \text{Activity number,} \\ \ell &= \frac{L_3}{L_1} : \text{Domain aspect ratio,} \end{aligned} \quad (22)$$

where  $\eta := \alpha_4$ .

In summary, the list of the model parameters is

$$\mathcal{P}_{\text{EL}} := \{\mathcal{R}_e, \mathcal{E}_r, \mathcal{A}, \ell, \alpha_i, \gamma_i\}. \quad (23)$$

Likewise,  $\{\tilde{v}, \mathbf{n}, \tilde{p}\}$  and the Lagrange multiplier  $\lambda$ , maintaining the unit director constraint, are the unknown fields of the Ericksen-Leslie model.

Since our work deals with the active liquid crystal confined in a channel, in a latter section we will recast the governing equations in terms of two space dimensions.

#### IV. SHEAR FLOW OF THE ERICKSEN-LESLIE MODEL

We suppress the superimposed bar notation and assume that all the variables are already dimensionless. We look for solutions such that the velocity field is unidirectional  $\mathbf{v} = (U(z, t), 0, 0)$  and the director angle  $\phi = \phi(z, t)$ . From equations (A1)-(A3), we get the reduced one-dimensional problem

$$\mathcal{R}_e \frac{\partial U}{\partial t} = -\frac{\partial p}{\partial x} + \ell^{-2} \frac{\partial}{\partial z} \left( g(\phi) \frac{\partial U}{\partial z} - \frac{1}{2} \mathcal{A} \ell \sin 2\phi \right), \quad (24)$$

$$0 = -\frac{\partial p}{\partial z} - 2\mathcal{E}_r^{-1} \ell^{-3} \frac{\partial}{\partial z} \left( \left( \frac{\partial \phi}{\partial z} \right)^2 \right) + \ell^{-2} \frac{\partial}{\partial z} \left( g_0(\phi) \frac{\partial U}{\partial z} - \mathcal{A} \ell \cos^2 \phi \right), \quad (25)$$

$$-\frac{\gamma_1 \ell^2}{2\alpha_4} \frac{\partial \phi}{\partial t} = \frac{\partial^2 \phi}{\partial z^2} + \frac{\mathcal{E}_r \ell}{4\alpha_4} \frac{\partial U}{\partial z} (-\gamma_1 + \gamma_2 \cos 2\phi), \quad (26)$$

where

$$g(\phi) = \frac{1}{4\alpha_4} (\alpha_1 \sin^2 2\phi + 2(\alpha_5 - \alpha_2) \cos^2 \phi + 2(\alpha_6 - \alpha_3) \sin^2 \phi + 2\alpha_4), \quad (27)$$

$$g_0(\phi) = \frac{1}{4\alpha_4} (\alpha_4 + 2\alpha_1 \sin 2\phi \cos^2 \phi + (\alpha_2 + \alpha_3 + \alpha_5 + \alpha_6) \sin 2\phi). \quad (28)$$

The function  $g(\phi)$  is the dimensionless form of the rate of dissipation  $\Delta$  of the flow:

$$g(\phi) = \alpha_4^{-1} \Delta > 0. \quad (29)$$

Next, we eliminate the pressure  $p$  from the equations of balance of linear momentum. Taking the partial derivative of equation (25) with respect to  $x$ , we get

$$0 = \frac{\partial^2 p}{\partial z \partial x}. \quad (30)$$

Likewise, taking the derivative with respect to  $z$  in equation (24) and applying to it the previous result, we get

$$\mathcal{R}_e \frac{\partial^2 U}{\partial z \partial t} = \ell^{-2} \frac{\partial^2}{\partial z^2} \left( g(\phi) \frac{\partial U}{\partial z} - \frac{1}{2} \mathcal{A} \ell \sin 2\phi \right). \quad (31)$$

Integrating once with respect to  $z$ , we get

$$\mathcal{R}_e \frac{\partial U}{\partial t} = \ell^{-2} \frac{\partial}{\partial z} \left( g(\phi) \frac{\partial U}{\partial z} - \frac{1}{2} \mathcal{A} \ell \sin 2\phi \right) + c_1(t), \quad (32)$$

where  $c_1(t)$  is arbitrary. The governing system reduces now to equations (26) and (32). Subsequent use of equation (25) determines the pressure.

##### A. Steady state flow

Let us now look for one-dimensional fields  $\mathbf{v} = (U(z), 0, 0)$ ,  $\phi = \phi(z)$  and  $s = s(z)$ . They satisfy the system of equations

$$0 = g(\phi) \frac{dU}{dz} - \frac{1}{2} \mathcal{A} \ell \sin 2\phi + c_1 z + c_2, \quad (33)$$

$$0 = \frac{d}{dz} \left( \frac{d\phi}{dz} \right) + \frac{\mathcal{E}_r \ell}{4\alpha_4} \frac{dU}{dz} (-\gamma_1 + \gamma_2 \cos 2\phi), \quad (34)$$

where  $c_1$  and  $c_2$  are arbitrary constants obtained in setting  $U_t \equiv 0$  in equation (32) and further integrating it with respect to  $z$ . Let us now determine the constants  $c_1$  and  $c_2$ . We point out that combining equation (24) in the steady state case with equation (33) yields

$$c_1 = -\ell^2 \frac{\partial p}{\partial x}.$$

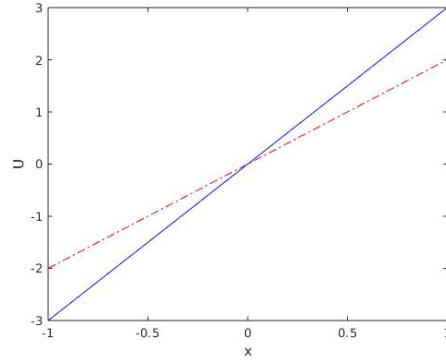


FIG. 2. Shear flow velocity profiles with shear rate 2 dimensionless units (red) and 3 (blue).

We shall take  $c_1 = 0$  which corresponds to the assumption that there is no applied external pressure gradient driving the flow. Furthermore, requiring that the velocity gradient vanishes when the activity is equal to zero implies that  $c_2 = 0$ . The resulting expression of the velocity gradient is then

$$U'(z) = \mathcal{A} \ell \sin(2\phi) / g(\phi), \quad (35)$$

Rewriting the previous equation in terms of the original dimensional variables, we get

$$v'_3(z) = \frac{\alpha L_1}{\eta V L_2} \sin(2\phi) / g(\phi), \quad (36)$$

where now the 'prime' notation indicates derivative with respect to the dimensional transverse variable,  $z$ , and  $\alpha$  denotes the activity parameter in (8). This indicates that the shear rate depends on the activity only but not on the width of the channel as observed in experiments<sup>10</sup>.

Substitution of equation (35) into (34) gives

$$0 = \frac{d}{dz} \left( \frac{d\phi}{dz} \right) + \frac{\mathcal{E}_r \mathcal{A} \ell^2}{4\alpha_4 g(\phi)} \sin 2\phi (-\gamma_1 + \gamma_2 \cos 2\phi). \quad (37)$$

Next, we look for solutions of equation (37) such that  $\phi$  and consequently  $U'(z)$  are constant. The latter corresponds to the observed states with linear velocity profile.

The angle of orientation of the director is

$$\cos(2\phi) = \frac{\gamma_1}{\gamma_2}. \quad (38)$$

From the properties of  $\gamma_1$  and  $\gamma_2$  (13) for rodlike nematics, we observe that  $\cos 2\phi < 0$  and so,

$$\frac{\pi}{4} < \phi < \frac{\pi}{2}.$$

That is, the angle  $0 \leq \frac{\pi}{2} - \phi \leq \frac{\pi}{4}$  between the director field and the horizontal direction is smaller than  $\frac{\pi}{4}$  radians,  $\frac{\pi}{2} > \frac{\pi}{2} - \phi > \frac{\pi}{4}$ . The velocity field is given by

$$U(z) = \mathcal{A} \ell g^{-1}(\phi) \sin(2\phi) z, \quad (39)$$

where the constant of integration has been chosen to give the odd profile. Rewriting the previous equation in terms of the original dimensional variables as in (36), we find that the velocity profile does not depend on the channel width. We observe that the solutions show very good agreement with the experimental results. Indeed, in the shear flow regimes, the activity parameter does not directly influence the flow alignment, but it does increase the velocity gradient, i.e., the shear rate.

Note that equation (38) shows that the director angle does not depend on the activity parameter  $\mathcal{A}$  whose dependence enters the expression (39) of the velocity gradient. Both properties are found to be in full agreement with experiments<sup>10</sup>.

## V. STABILITY ANALYSIS

From henceforth, we study the stability of the solution  $(U(z), \phi_0)$  under perturbations of the form

$$\begin{aligned}\tilde{v}_1 &= U + \epsilon v_1(t, x, z), \\ \tilde{v}_3 &= \epsilon v_3(t, x, z), \\ \tilde{\phi} &= \phi_0 + \epsilon \phi_1(t, x, z),\end{aligned}$$

where  $U$  in (39) and  $\phi_0$  in (38) are the shear base flow solution and  $s_0$  and  $\phi_0$  are constant. Substituting these expressions into the full two-dimensional system of governing equations (A1), (A2) and (A3), we obtain the linear system (B1), (B2) and (B3) for the fields  $(v_1(t, x, z), v_3(t, x, z), \phi_1(t, x, z))$ .

Moreover, we propose the following exponential expressions of the unknown fields, consistent with those used in the normal mode stability analysis:

$$\Psi(t, x, z) = \psi(z)e^{i\omega(x-ct)} \quad (40)$$

$$v_1(t, x, z) = \frac{\partial \Psi}{\partial z} = e^{i\omega(x-ct)} \frac{d\psi}{dz} \quad (41)$$

$$v_3(t, x, z) = -\frac{\partial \Psi}{\partial x} = -i\omega\psi(z)e^{i\omega(x-ct)}, \quad (42)$$

where  $\Psi$  denotes the stream function of the flow. Also, for the direction angle, we assume that

$$\phi_1(t, x, z) = \Phi(z)e^{i\omega(x-ct)}. \quad (43)$$

Here,  $\omega$  and  $c$  are dimensionless complex numbers corresponding to the spatial frequency and to the speed or growth of the perturbation, respectively. Specifically, separating  $\Psi$  and  $\Phi$  into their real and imaginary parts, it follows that  $\text{Re}(\omega)$  represents the spatial oscillatory part of the perturbation and  $\text{Im}(c)$  corresponds to its time growth rate. From now on, we will restrict ourselves to the case when

$$\text{Im}(\omega) = 0.$$

Substituting the expressions (40)-(43) into the linear governing equations (B1), (B2) and (B3), we obtain a linear system (C3) and (C4) for the new variables. Specifically the former is a fourth order linear ordinary differential equation for  $\psi$  and the latter is a second order equation for  $\Phi$ .

A relevant quantity in the analysis of flow which also helps quantify the transition to turbulence is the vorticity vector:  $\mathbf{W} = \nabla \times \mathbf{v}$ . Since we are dealing with two-dimensional flow, it reduces to a scalar,

$$W(x, z) = \frac{\partial v_1}{\partial z} - \frac{\partial v_3}{\partial x} = e^{i\omega(x-ct)} \left[ \frac{d^2\psi}{dz^2} - \omega^2\psi(z) \right]. \quad (44)$$

The governing equations for the perturbations are given by (C3) and (C4) in the Supplementary Materials section, where their derivation is carried out.

We require that the perturbations do not change the boundary values of the velocity and alignment of the basic solutions. That is, we impose the conditions

$$\psi(\pm 1) = 0, \quad (45)$$

$$\psi'(\pm 1) = 0, \quad (46)$$

$$\Phi(\pm 1) = 0. \quad (47)$$

## VI. THE NUMERICAL METHOD

The Chebyshev polynomials<sup>18,19</sup> in the variable  $z$  form an orthogonal family on  $z$ -interval  $[-1, 1]$ . We apply the Chebyshev-QZ algorithm<sup>3,2</sup> to solve the generalized eigenvalue problem (45), (46), (47) (C3) and (C4). We first

approximate the stream function  $\psi(z)$  and angle function  $\Phi(z)$  by the truncated Chebyshev expansions

$$\psi(z) = \sum_{n=0}^N a_n T_n(z), \quad \Phi(z) = \sum_{n=0}^{N-2} b_n T_n(z), \quad (48)$$

where  $T_n(z)$  denotes the  $n$ -th order Chebyshev polynomial of the first-kind. Our goal is to determine the coefficients  $a_n$ ,  $b_n$  and the eigenvalue  $c$ . To keep the unknown coefficients evenly distributed over the two functions, we choose different orders of truncations for  $\psi(z)$  and  $\Phi(z)$ . We collocate the Galerkin truncation at the extrema of the Chebyshev polynomial

$$z = \cos\left(\frac{j\pi}{N-2}\right), j = 1, \dots, N-3 \quad (49)$$

Thus, evaluating the governing equations at these extrema points, we obtain  $2N - 6$  linear algebraic equations. Six additional relations are provided by the corresponding boundary conditions (45)-(47), which complete the system.

The substitution of the truncated expansions (48) into the boundary conditions yields rows of zeros, which produce a spurious eigenvalue<sup>3</sup>, and therefore, we eliminate them. The full system of equations becomes the algebraic eigenvalue problem

$$[A_R + iA_I] \mathbf{x} = c[B_R + iB_I] \mathbf{x} \quad (50)$$

where  $\mathbf{x} = (a_3, \dots, a_N, b_2, \dots, b_{N-2})^T \in \mathbb{C}^{2N-5}$ ,  $A_R$ ,  $A_I$ ,  $B_R$  and  $B_I$  denote  $(2N - 5) \times (2N - 5)$  real matrices. Using the QZ-algorithm of MATLAB, we obtain the eigenvalues and corresponding eigenvectors. Details of the steps leading to the system (50) are given by equations (E1)-(E2) and (E3) in the supplementary material.

We end this section by listing the values of the Leslie viscosity coefficients used in the simulations. For extensile liquid crystals, we take

$$\alpha_1 = 0, \alpha_2 = -1.5, \alpha_3 = -0.5, \alpha_4 = 2, \alpha_5 = 2, \alpha_6 = 0, \gamma_1 = 1, \gamma_2 = -2. \quad (51)$$

The data list to be used in the simulations of contractile liquid crystals is

$$\alpha_1 = 0, \alpha_2 = -1.5, \alpha_3 = -0.5, \alpha_4 = 4, \alpha_5 = -2, \alpha_6 = 0, \gamma_1 = 1, \gamma_2 = 2. \quad (52)$$

These provide simple values that still maintain the anisotropy of the viscosity, satisfy the positivity of the rate of dissipation function, and also represent the aligning regime in each class. Moreover, we take the constant order parameter as  $s_0 = 1.0$ .

The numerical study yields plots of  $\omega$  with respect to the  $\mathcal{A}$ , for different values of  $\mathcal{E}_r$ ,  $\ell$  and  $\mathcal{R}_e$ , showing regions of the spatial frequency domain for which the corresponding perturbation is either stable or unstable, that is, whether it decays or grows in time. The study also yields plots of the streamlines, vorticity and director angle of the perturbation fields. The tangent vector field of the former corresponds to the velocity field of the system. We focus in quantitatively understanding the role of the parameter values in determining the instability behavior. Specifically, we assume that the Leslie coefficients  $\alpha_i$  are fixed and seek how the dimensionless parameters  $\mathcal{E}_r$ ,  $\mathcal{A}$ ,  $\ell^2$  and  $\mathcal{R}_e$  affect the stability of the shear flow.

Our analysis follows along the lines of many previous investigations of the physical mechanisms that cause either instability or stability in terms of eigenmodes of the linearized system<sup>8</sup> and<sup>17,4</sup>. To characterize the stability of the shear flow steady state, we check the growth rate of the dominant unstable eigenmode of the perturbation that affects the system. For unstable systems, the largest value of the linear growth rate and the corresponding wavenumber excite the system and modify the basic state in some essential fashion. On the other hand, stable perturbation modes also modify the system but decay in time.

## VII. STABILITY ANALYSIS

In this section, we perform a stability analysis of the basic shear flow solution for extensile fibers, that is, in the case  $\mathcal{A} > 0$ . For this, we solve the system (50) following the method presented in Section VI. The result of the analysis is presented in the graphs of figures 3-9. Figures 10 and 11 show the profiles of the perturbing fields. We summarize the results of the computations as follows.

- The main general trend is that increasing, either one of the quantities  $\mathcal{E}_r$ ,  $\ell$  or  $\mathcal{A}$ , prompts unstable behavior of the system.

- In particular, Fig. 3 shows that, for fixed  $\mathcal{E}_r = 100$  and  $\mathcal{R}_e = 5$ , the critical value of the activity number  $\mathcal{A}$ , above which the system becomes unstable, decreases with  $\ell$ , with  $\mathcal{A}_c \approx 250$  dimensionless units, for  $\ell = 0.1$ ,  $\mathcal{A}_c \approx 100$ , for  $\ell = 0.2$ , and  $\mathcal{A}_c \approx 20$  for  $\ell = 0.3$ .
- Fig. 4(a) shows the analogous behavior but with respect to increasing  $\mathcal{E}_r$ . The increase of  $\mathcal{E}_r$ , while keeping the other parameter fixed, also promotes unstable behavior. For  $\mathcal{R}_e = 0.1$ ,  $\ell = 0.2$  the threshold values of  $\mathcal{A}$  above which the flow becomes unstable are found to be  $\mathcal{A} \approx 950$  for  $\mathcal{E}_r = 100$ ,  $\mathcal{A} \approx 200$  for  $\mathcal{E}_r = 500$  and  $\mathcal{A} \approx 100$   $\mathcal{E}_r = 1000$ .
- Fig.5 shows that increasing  $\mathcal{R}_e$  may not decrease the critical activity number threshold leading to instability, but it does increase the unstable frequency range as shown in Figure 5(b). Figure 5(c) reiterates the role of the channel width in promoting instability, showing the instability threshold of  $\mathcal{A} \approx 100$ , even for  $\mathcal{R}_e = 5$  and  $\mathcal{E}_r = 250$  but with  $\ell = 0.4$ .
- Fig. 8 shows the growth rate given by  $\max \text{Im}(c)$  with respect to  $\mathcal{A}$ , for the wave lengths  $\omega = 50, 75$ , and  $100$ . The remaining parameters are chosen as  $\mathcal{R}_e = 5$ ,  $\mathcal{E}_r = 1000$   $\ell = 0.2$ . We find that the system is stable ( $\max \text{Im}(c) < 0$ ) for small  $\mathcal{A}$ , with a stability threshold between  $\mathcal{A} = 100$  (for  $\omega = 50$ ) and  $\mathcal{A} = 150$  (for  $\omega = 100$ ) dimensionless units. For small frequencies, the growth rate shows a parabolic profile, reaching a maximum whose  $\mathcal{A}$ -location increases with frequency, with a possible return to stability at higher  $\mathcal{A}$ . For instance, for  $\omega = 50$ , the system changes from stable to unstable at  $\mathcal{A} \approx 100$ , and then regaining stability at  $\mathcal{A} \approx 500$ . This behavior is also reflected in Fig. 3(b). The profile becomes linear at  $\omega = 100$ .
- Fig. 9 shows the graphs of the growth rate with respect to the frequency, at three different activity values,  $\mathcal{A} = 150, 200, 250$ . We observe the nonconvex shape of the graphs, for small frequencies, reaching a positive maximum. All the graphs tend to neutral stability, with increasing  $\omega$ , following a profile nearly independent of  $\mathcal{A}$ .
- Figures 10 illustrate the form of the perturbation fields that contribute to the shear flow. We present contour plots of the stream function, the angle and the vorticity contour (Fig. 11).

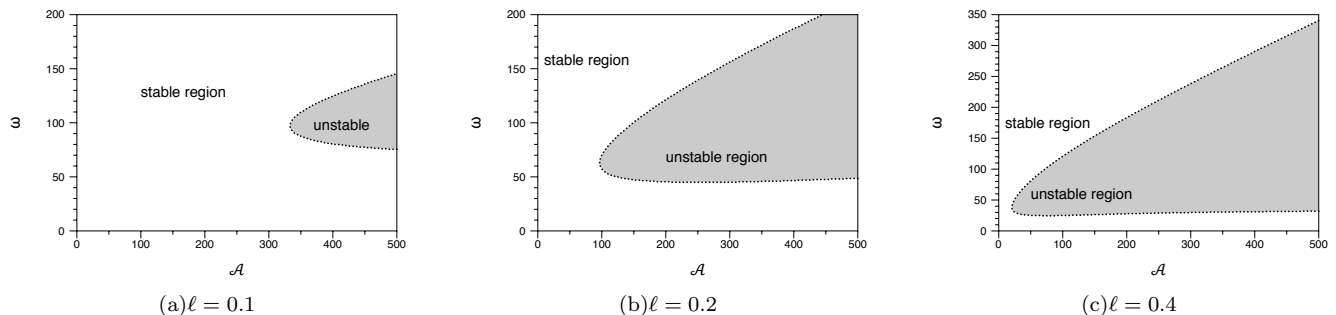


FIG. 3. Regions of stability in the  $\mathcal{A}\omega$ -plane for different channel ratios. The black dotted curve separates the stable and unstable regions in the plane. In all three plots  $\mathcal{R}_e = 5$  and  $\mathcal{E}_r = 1000$ .

## VIII. CONCLUSION

This article examines the onset of instability of a uniformly aligned shear flow of active extensile fibers in a confined channel. The results point to a transition towards turbulent regimes as the width of the channel or the level of activity increase. The follow up work will examine the observed pairwise,  $(\pm \frac{1}{2})$  defect elimination that accompanies the transition to turbulence.

## SUPPLEMENTARY MATERIALS

See the supplementary materials for detailed derivation of model equations and numerical implementations.

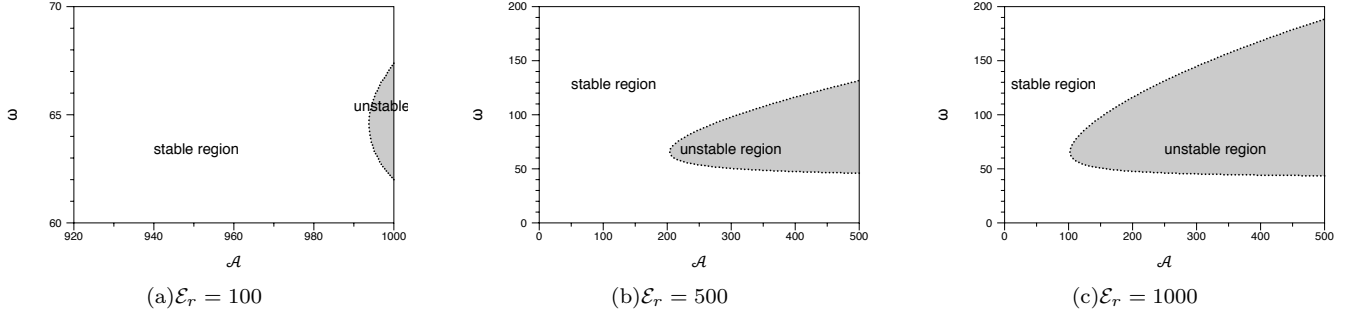


FIG. 4. Regions of stability in the  $\mathcal{A}\omega$ -plane, with the black dotted curves having the same meaning as in Figure 3. These plots correspond to  $\mathcal{R}_e = 0.1$  and  $\ell = 0.2$ .

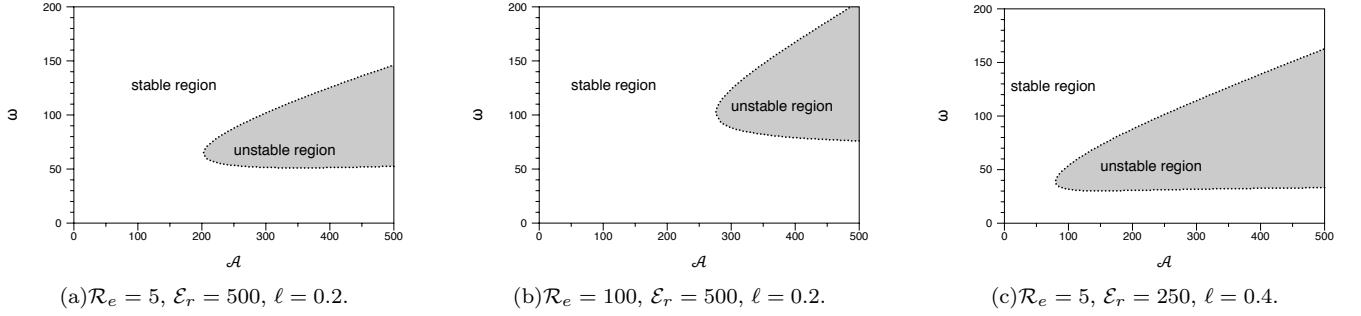


FIG. 5. Regions of stability in the  $\mathcal{A}\omega$ -plane, with the black dotted curves having the same meaning as in Figure 3. Plot 5(c) corresponds to  $\mathcal{R}_e = 5, \mathcal{E}_r = 250$  and  $\ell = 0.4$  to compare with Fig. 3(c).

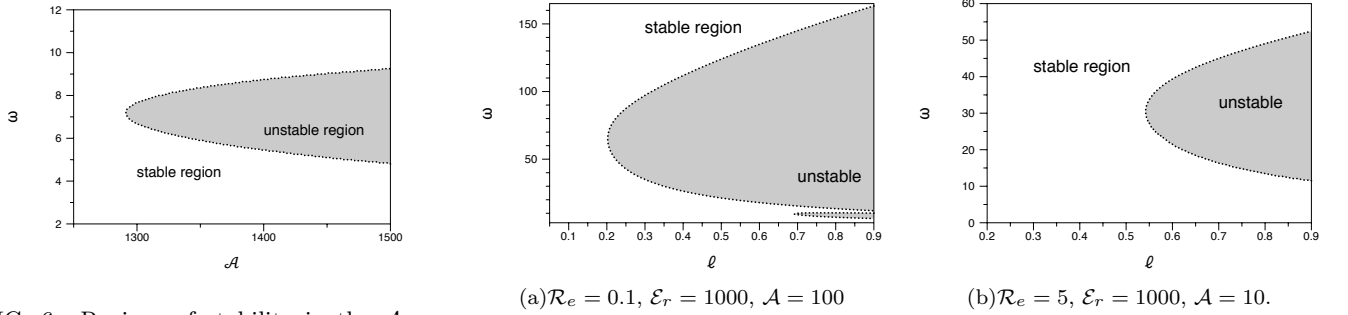


FIG. 6. Regions of stability in the  $\mathcal{A}\omega$ -plane, with the black and dotted curves having the same meaning as in Fig. 3.  $\mathcal{R}_e = 100$  and  $\ell = 0.2$ .

FIG. 7. Stability diagrams in  $\ell\omega$ -plane

## ACKNOWLEDGMENT

M.C Calderer gratefully acknowledges the support of the National Science Foundation through grants DMS-1435372 and DMS-DMREF 1729589. L. Yao thanks the support of the National Science Foundation DMS 1852597. L. Zhao thanks the support of AWM-NSF mentor grant.

## DATA AVAILABILITY STATEMENT

There is no experimental data involved in this study. The numerical algorithm is available in the supplementary documents. The code for generating figures that support the findings of this study will be available from the corresponding author upon reasonable request.

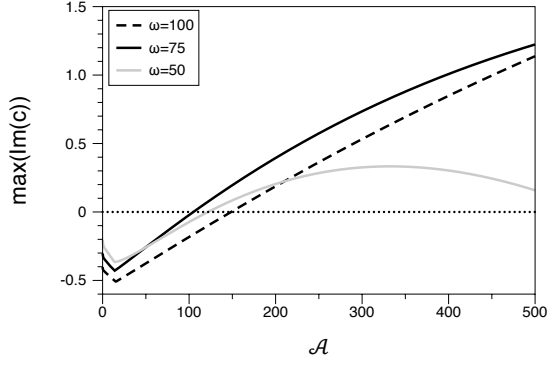


FIG. 8. Growth rate of the maximum imaginary part of eigenvalue  $c$  with the dotted lines at zero. The perturbation wave lengths are fixed as  $\omega = 50, 75, 100$ , and  $\mathcal{R}_e = 5$ ,  $\mathcal{E}_r = 1000$   $\ell = 0.2$ .

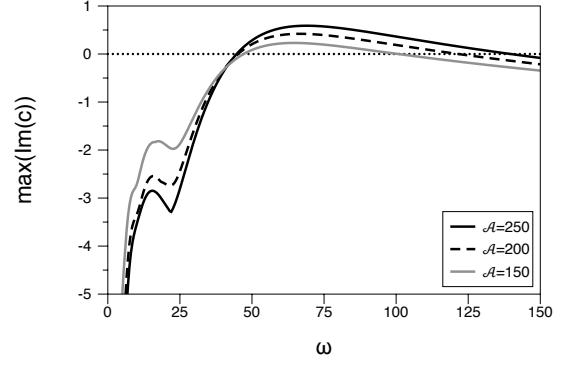


FIG. 9. Growth rate of the maximum imaginary part of eigenvalue  $c$  with the dotted lines at zero. The active parameters are fixed at three values  $\mathcal{A} = 150, 200, 250$ . For these results,  $\mathcal{R}_e = 5$ ,  $\mathcal{E}_r = 1000$  and  $\ell = 0.2$ .

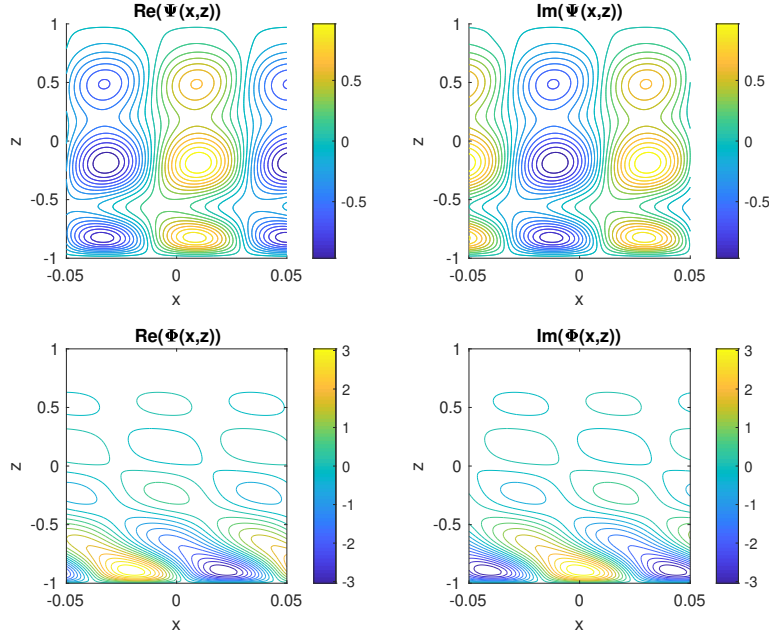


FIG. 10. Contour plots for the stream function  $\Psi(x, z)$  and order parameter  $\Phi(x, z)$  of a sample unstable perturbation mode.  $\omega = 75$ ,  $\mathcal{R}_e = 5$ ,  $\mathcal{E}_r = 1000$ ,  $\mathcal{A} = 200$ , and  $\ell = 0.2$ .

- <sup>1</sup>D Baals and Siegfried Hess. The viscosity coefficients of oriented nematic and nematic discotic liquid crystals; affine transformation model. *Zeitschrift für Naturforschung A*, 43(7):662–670, 1988.
- <sup>2</sup>D Bourne. Hydrodynamic stability, the Chebyshev tau method and spurious eigenvalues. *Continuum Mechanics and Thermodynamics*, 15(6):571–579, 2003.
- <sup>3</sup>J.J. Dongarra, B. Straughan, and D.W. Walker. Chebyshev tau-qz algorithm methods for calculating spectra of hydrodynamic stability problems. *Applied Numerical Mathematics*, 22(4):399 – 434, 1996.
- <sup>4</sup>PG Drazin, LN Howard, and GG Chernyi. *Advances in applied mechanics*, 1966.
- <sup>5</sup>G Duclos, C Blanch-Mercader, V Yashunsky, G Salbreux, J-F Joanny, J Prost, and Pascal Silberzan. Spontaneous shear flow in confined cellular nematics. *Nature physics*, 14(7):728–732, 2018.
- <sup>6</sup>Brian J Edwards, Antony N Beris, and Miroslav Grmela. Generalized constitutive equation for polymeric liquid crystals part 1. model formulation using the hamiltonian (poisson bracket) formulation. *Journal of non-newtonian fluid mechanics*, 35(1):51–72, 1990.
- <sup>7</sup>S. A. Edwards and J. M. Yeomans. Spontaneous flow states in active nematics: A unified picture. *EPL (Europhysics Letters)*, 85(1):18008, jan 2009.
- <sup>8</sup>A. E. Fraser, P. W. Terry, E. G. Zweibel, and M. J. Pueschel. Coupling of damped and growing modes in unstable shear flow. *Physics of Plasmas*, 24(6), 6 2017.

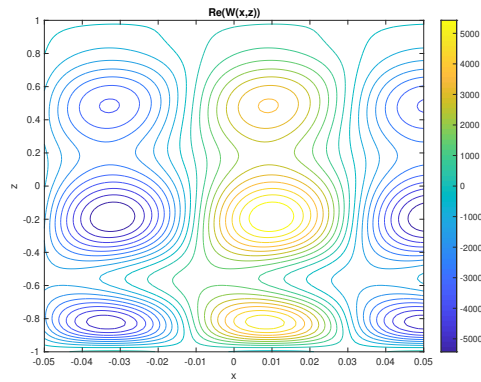


FIG. 11. The vorticity field  $\text{Re}(W(x, z))$  of the sample unstable perturbation mode in Fig. 10.

- <sup>9</sup>Pau Guillamat, Jordi Ignés-Mullol, and Francesc Sagués. Taming active turbulence with patterned soft interfaces. *Nature communications*, 8(1):1–8, 2017.
- <sup>10</sup>Jérôme Hardoüin, Rian Hughes, Amin Doostmohammadi, Justine Laurent, Teresa Lopez-Leon, Julia M. Yeomans, Jordi Ignés-Mullol, and Francesc Sagués. Reconfigurable flows and defect landscape of confined active nematics. arXiv:1903.01787, xx(x):xx, 2019.
- <sup>11</sup>Frank M Leslie. Continuum theory for nematic liquid crystals. *Continuum Mechanics and Thermodynamics*, 4(3):167–175, 1992.
- <sup>12</sup>Frank Matthews Leslie. Some thermal effects in cholesteric liquid crystals. *Proceedings of the Royal Society of London. Series A. Mathematical and Physical Sciences*, 307(1490):359–372, 1968.
- <sup>13</sup>M. C. Marchetti, J. F. Joanny, S. Ramaswamy, T. B. Liverpool, J. Prost, Madan Rao, and R. Aditi Simha. Hydrodynamics of soft active matter. *Rev. Mod. Phys.*, 85:1143–1189, Jul 2013.
- <sup>14</sup>D. Marenduzzo, E. Orlandini, and J. M. Yeomans. Hydrodynamics and Rheology of Active Liquid Crystals: A Numerical Investigation. *Physical Review Letters*, 98(11):118102, March 2007.
- <sup>15</sup>Sriram Ramaswamy. The mechanics and statistics of active matter. *Annual Review of Condensed Matter Physics*, 1(1):323–345, 2010.
- <sup>16</sup>Tim Sanchez, Daniel TN Chen, Stephen J DeCamp, Michael Heymann, and Zvonimir Dogic. Spontaneous motion in hierarchically assembled active matter. *Nature*, 491(7424):431–434, 2012.
- <sup>17</sup>Geoffrey Ingram Taylor. Viii. stability of a viscous liquid contained between two rotating cylinders. *Philosophical Transactions of the Royal Society of London. Series A, Containing Papers of a Mathematical or Physical Character*, 223(605-615):289–343, 1923.
- <sup>18</sup>Kim-Chuan Toh and Lloyd N Trefethen. The chebyshev polynomials of a matrix. *SIAM Journal on Matrix Analysis and Applications*, 20(2):400–419, 1998.
- <sup>19</sup>Lloyd N Trefethen. *Spectral Methods in MATLAB*. SIAM: Society for Industrial & Applied Mathematics, 2001.
- <sup>20</sup>R Voituriez, Jean-François Joanny, and Jacques Prost. Spontaneous flow transition in active polar gels. *EPL (Europhysics Letters)*, 70(3):404, 2005.